Optics Communications 454 (2020) 124364

Contents lists available at ScienceDirect

Optics Communications

journal homepage: www.elsevier.com/locate/optcom

Design of 45° periscopic visual field expansion device for peripheral field loss

Hee-Jin Choi [a], Eli Peli [b], Minyoung Park [a], Jae-Hyun Jung [b,*]

[a] Department of Physics and Astronomy, Sejong University, Seoul 05006, Republic of Korea

[b] Schepens Eye Research Institute, Massachusetts Eye and Ear, Department of Ophthalmology, Harvard Medical School, Boston, MA, USA

ABSTRACT

Patients with visual field loss have difficulty in mobility due to collision with pedestrians/obstacles from the blind side. In order to compensate for the visual field loss, prisms which deflect the field from the blind to the seeing side, have been widely used. However, the deflection power of current clinical Fresnel prisms is limited to ~30° and only allows a 5° eye scanning range to the blind side. This is not sufficient to avoid most collisions and results in demands for a device with a higher power. In this paper, we propose a novel design and optimization of a higher power prism-like device (cascaded structure of mirror pairs filled with refractive medium) and verify enhanced field expansion of up to 45° in optical ray tracing and photorealistic simulations.

Patients with visual field loss report collisions with other pedestrians/objects and tripping over obstacles, and are commonly not permitted to drive. All of these factors severely restrict their mobility and quality of life. Peripheral visual field loss, tunnel vision (severe peripheral field constriction to <20° of residual central field), maybe due to retinal diseases such as retinitis pigmentosa, choroideremia, and advanced glaucoma [1,2]. The loss of half of the visual field in both eyes on the same side (Homonymous hemianopia, HH), which is a common peripheral field loss, can be caused by brain injuries such as stroke, trauma, or tumors [3–6].

Among various efforts to help the patients with visual field loss as described above, prism glasses have been long considered one of the simplest, most effective, and helpful devices for field expansion, shifting (deflecting) the field from the blind side (prism base side) to the seeing side. Peripheral prism glasses [4] to avoid confusions in the central visual field were established as an effective field expansion device for field loss patients in walking [2] and driving [7]. It is obvious that larger deflection power can deliver more visual information from farther blind side to the seeing side of patients with visual field loss, devices with higher prism power (deflection power).

Peli et al. [8] found that the collision risk with other walking pedestrian increases with eccentricity, and peaks at 45°. Thus, visual field expansion to 45° is desirable to effectively reduce the risk of collision. However, current clinically available prism glasses provide only up to ~30° field expansion with 57Δ (prism diopter) Fresnel prisms [9]. In addition, supporting wider eye scanning range (up to the 15° range of most eye movements [10]) into the blind side and better image quality [9] are also desirable.

The main effect that restricts the optical power of conventional prism is the total internal reflection (TIR). The current clinically available 57Δ prism allows only 5° eye scanning range into the blind side due to the TIR [6], which is far less than the maximal eye movements range of 15° mentioned above. TIR limits the rated prism power (measured at the normal incidence) higher than 41° as shown in Fig. 1(a) and (b).

Though it is possible to move the TIR limit farther by using angle of smaller deviation in the prism, this results in smaller field expansion [6]. The images seen through the prism when approaching the TIR limitation are highly distorted (minified) and dimmer [6]. Color dispersion in prisms lowers the image quality further as it reduces contrast [11]. When using Fresnel prisms to reduce the size and weight of high power prisms in current clinical prism glasses, light scattered at the non-imaging base surface further reduces image quality [6,11]. The reduced image quality may significantly affect hazard detection through the prism.

There is a need for a device which provides higher optical power, wider eye scanning range, and less distortion. Previously, we proposed a concept of higher power mirror prism-like element [9], which is a cascaded structure of mirror periscopic prism (MP). An MP deflects the light path through double reflections, and the device's (deflection) power is simply double the apex angle (the angle between mirrors) as shown in Fig. 1(c) and (d). The reflective deflection from an MP is free of refractive image degradations such as distortion, transmittance reduction, color dispersion, and TIR (Fig. 1d) [9]. MP does not have a physical base and apex, but we name them to match with the physical base and apex in the conventional prism and thus the deflection direction. The conceptual design in our previous work [9] has not achieved the practical goal of 45° optical power and 60° field of view (FoV) due to the limitation that the sizes of mirrors increase in order to provide more optical power and FoV as shown in Fig. 1(d). An MP with higher power requires impractically longer mirrors.

In this paper, we analyze the requirements of the cascaded MP modules and propose a new MP design filled with polymethyl methacrylate

* Corresponding author.
E-mail address: jaehyun_jung@meei.harvard.edu (J.-H. Jung).

https://doi.org/10.1016/j.optcom.2019.124364
Received 26 May 2019; Received in revised form 6 August 2019; Accepted 9 August 2019
Available online 13 August 2019
0030-4018/

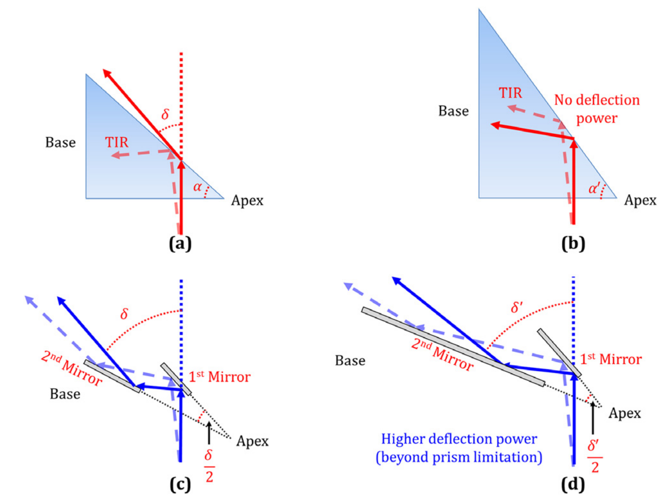

Fig. 1. Limitation of conventional and reflective prisms. (a) Limitation of a conventional prism. In a conventional PMMA prism with an apex angle (α), maximal deflection power (δ) is ~41° (50% transmittance) with no eye scanning range toward the blind side of HH (dashed arrow). (b) Due to the TIR, higher apex angle (α') does not result in higher deflection power even at the normal incidence. (c) Principle of a double reflective deflection in an MP. The reflective deflection power (δ) of an MP is double the apex angle ($\delta/2$). (d) The MP can provide higher deflection power (δ') with a higher apex angle ($\delta'/2$) with no limitation of TIR, but it requires longer mirrors.

(PMMA) to hold the structure and provide refractive power. The new MP design provides a higher deflection power of 45° by combining the low refractive and high reflective deflection powers in practical sizes. It also provides FoV up to ~57° (42° seeing FoV and 15° eye scanning range) for normal eye scanning range in HH [5].

We derive Eqs. (1)–(4) for the design of the cascaded MP modules with reflective deflection power, δ_{M_n}. The main parameters of cascaded MP modules (Fig. 2) are the size of mirrors (M_n) and the distance between MP modules and the center of the entrance pupil of the eye (D_n). We denote the FoV of each module and the angle of the 1st reflection from the mirror surface as θ_n and β_n, respectively. Since the MP modules abut each other in the cascade structure in order to prevent the blocking of light paths from neighboring modules, the derived equations also have the form of series equations. For patients with left HH, the left side mirror of the nth MP module should be the right side mirror of the $(n+1)$th MP module as shown in Fig. 2. The relationship between the length of the mirror (M_n) and the distance to the mirror (D_n) is derived as follows.

$$\beta_{n+1} = \beta_n + \frac{\delta_{M_n}}{2} - \theta_n, \tag{1}$$

$$D_{n+1} = D_n \frac{\sin 2\beta_n}{\sin(2\beta_n - \theta_n)}, \tag{2}$$

$$M_1 = D_1 \frac{\sin\theta_1}{\sin(\beta_1 - \theta_1)}, \tag{3}$$

$$M_{n+1} = D_n \frac{\sin\theta_n \sin\beta_n \sin 2(\beta_n - \theta_n)}{\sin(\beta_n - \theta_n)\sin(2\beta_n - \theta_n)\sin(\beta_n - \theta_n - \frac{\delta_{M_n}}{2})} \tag{4}$$

Eq. (4) also shows that a single MP module with 45° prism power and 60° FoV requires an impractical 3.7 m mirror (M_2) placed 5 mm from the eye (D_2) with 82.5° of β_2. A cascade of MP modules is, therefore, required for practically small and safe design. We set design constraints that M_n and D_n should be less than 20 mm and larger than 16 mm (typical distance from the center of the entrance pupil of the eye to the back surface of a corrective lens [12]), respectively.

The shaded area in Fig. 3 shows the combinations of β and θ that satisfy the safety consideration of $D_{n+1} \geq D_n$ and physical consideration

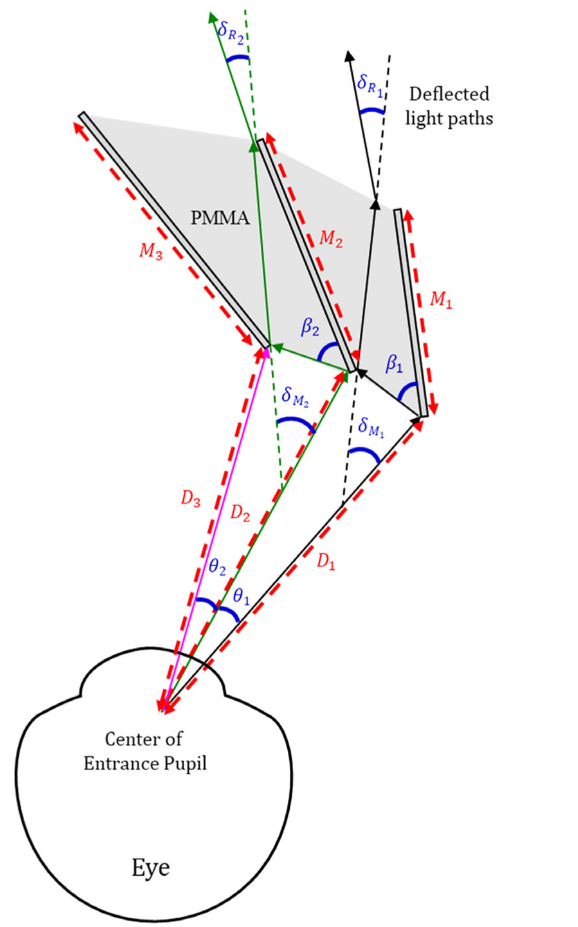

Fig. 2. Parameters of cascaded MP modules. D_n is the distance between the edge of the mirror and the entrance pupil of the eye, and Mn the size of the nth mirror. The FoV of each module is θ_n. Parameters β_n, δ_{M_n}, and δ_{R_n} are the angle of the 1st reflection from the mirror surface, reflective deflection power, and refractive deflection power, respectively. Total deflection power (δ) is sum of δ_R and δ_M.

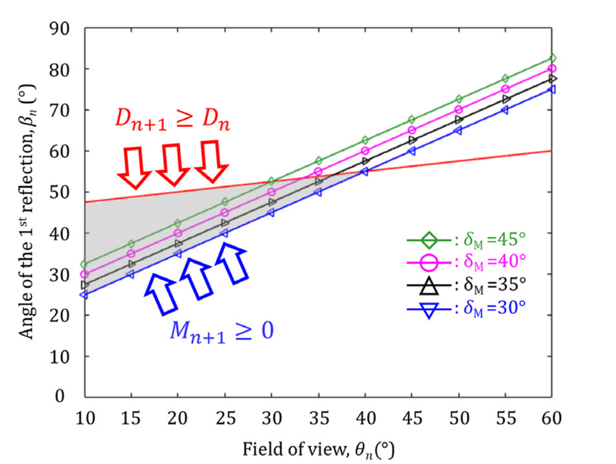

Fig. 3. Relations between β_n and θ_n. The shaded area satisfies both the safety ($D_{n+1} \geqslant D_n$) and physical ($M_{n+1} \geqslant 0$) considerations.

of $M_{n+1} \geq 0$ for various δ_{M_n} from 30° to 45°. The relation to satisfy the consideration of $M_{n+1} \geq 0$ is $\sin(\beta_n - \theta_n - (\delta_{M_n}/2)) \geq 0$ since all the other terms in Eq. (4) are positive. The graph shows that the angle of the 1st reflection (β) is restricted by the FoV in a single MP module to satisfy the above requirements.

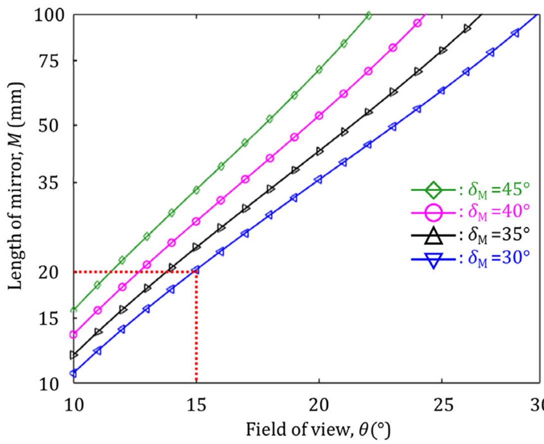

Fig. 4. Practical limitation ($M_{n+1} \leqslant 20$ mm) for a single MP, which leads to a single MP with less than 15° FoV (θ). Note that M is in log scale.

We derived the restriction of FoV (θ) from the practical constraint of $M_{n+1} \leq 20$ mm as shown in Fig. 4 with the same range of δ_M. The analysis shows that the size of mirror M is increasing steeply with θ. If δ_M increases, the size of mirror M should be much larger than the practical limitation. Thus, we found that the FoV of a single MP should be less than 15° to meet the practical limit even if δ_M is 30°. Therefore, at least four MP modules are necessary to achieve the overall field of ≈60°.

Though the basic design rule has been derived through the analyses above for an MP with $\delta_M = 30°$, it is still necessary to further increase δ_M while keeping the practical limitation of $M_{n+1} \leq 20$ mm and the safety requirement of $D_n \geq 16$ mm, as noted above. To achieve that goal, we propose a design where the cascaded MP modules have the combined total deflection power δ from differently distributed reflective (δ_{M_n}) and refractive (δ_{R_n}) deflection powers. We filled the space between mirrors with a refractive medium (PMMA, refractive index = 1.49) which provides additional flexibility of design by allowing us to control δ_{R_n}.

The main idea is giving the MPs lower δ_{M_n} in order to limit the mirror sizes. Then, the cascade structure enforcing an increase of the mirror size ($M_{n+1} < M_n$) makes the PMMA between the mirrors form a prism shape at the exit window of the MPs with δ_R. Additional control of δ_{R_n} is available by changing the mirror size M_n slightly. The effect on the image quality from the refraction is negligibly small due to the small angle of incidence at the surface [4]. With these principles, we designed a device with FoV of 57.1° and deflection power of approximately 45° while satisfying the practical and safety considerations. The parameters have been slightly different from the preliminary calculations based on Eqs. (1)–(4) as the δ_{R_n} has been added by iterative changes of mirror sizes, and all MP modules satisfy both the dimensional and optical requirements. Table 1 shows the detailed parameters of the four cascaded MP modules. Note that it is possible to achieve a higher refractive power δ_{R_n} as M_n is increased due to the cascaded structure. Thus, refractive power δ_{R_n} should be adjusted in order to maintain the total deflection power of 45°.

We performed a ray-tracing simulation using LightTools (Synopsis, Mountain View, CA) to verify the field expansion through the proposed design. The dimension of the designed MP is 36 mm × 16 mm × 8 mm (W × D × H), respectively. The calculated total deflection powers δ_n of each module are shown in Fig. 5. Though there are small tunnel scotomas [13] between modules, their effects are negligible (< 0.1°) at the distances of objects of interest in mobility. The variation in deflection powers between modules due to the additional refractive prism structure (δ_{R_n}) was about 1°.

We illustrated the image quality and field expansion in the perceived scene. Since there is no way to visualize and compare the

Table 1
Specification of cascaded MP design with FoV of 57.1° (42.1° in seeing FoV and 15° for eye scanning range) and total deflection power of approximately 45°. Note that each module consists of parameters from two mirrors (M and D) and angular parameters between them (θ and δ).

Module#	M (mm)	D (mm)	θ (°)	δ_M (°)	δ_R (°)	δ (°)
1	10.7 12.8	20 19.6	12	30	12.9	42.9
2	12.8 15.4	19.6 18.6	13.5	33.8	10.6	44.4
3	15.4 17.8	18.6 16.9	15	37.5	7.7	45.2
4	17.8 19.3	16.9 16.9	16.6	41.5	3.8	45.4

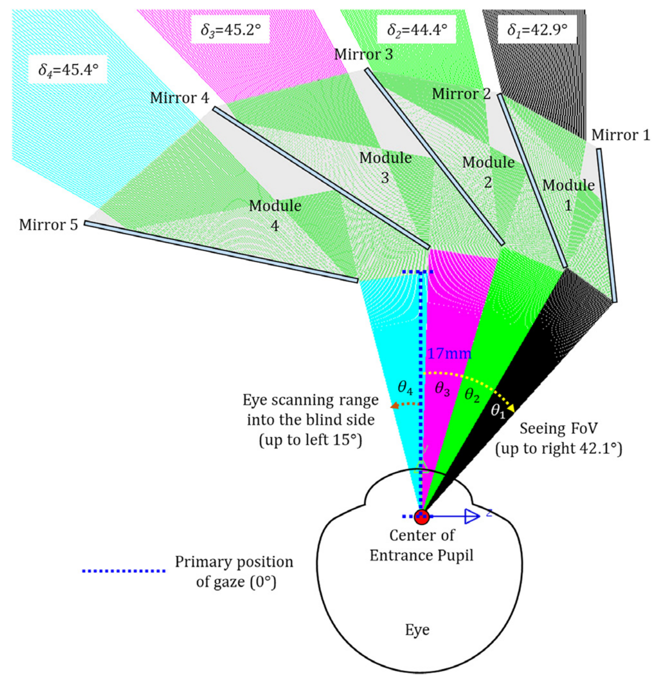

Fig. 5. Ray tracing of the new MP design for left HH. Different colors mark rays in each module (~15° FoV). The deflection powers of the central ray in each MP module (δ_n) are matched with the designed values. Tunnel scotoma (gaps between ray bundles) is negligible in the practical distance.

perceived scene by a patient with HH, the effects of MP and conventional Fresnel prism with vertical size of 8 mm (conventional peripheral prisms [5,6]) were compared using photorealistic rendering with a virtual pinhole camera in LightTools. We used a pinhole camera simulation with finite pupil to clearly illustrate the size of FoV and amount of the shift without blur effects in the boundaries of the MP. In the simulation, a flat virtual image wall has been set at 6 m from the flat virtual camera sensor (simulated eye) to cover 120° of the visual field. At the virtual wall, an image composed of a pattern of vertical lines (Fig. 6(a)) was mapped to illustrate the total deflection power and the transmittance for the designed MP shown in Fig. 6(b). We also modeled a conventional 57Δ Fresnel prism in PMMA with a 38.5° apex angle, and each segment had a 0.35 mm width for comparison. The size of the 57Δ Fresnel prism was 16.4 mm in order to cover 28.8° FoV (57Δ) in the seeing side and 15° in the blind side.

Fig. 6 illustrates the differences in visual field expansion and image quality between the MP and the Fresnel prism. A perceived view through the MP is shown in Fig. 6(b). The simulation shows an expansion of 45° without distortion and high transmittance. About 15° of eye scanning range enables the MP to provide a total FoV of 57° as designed. In contrast, conventional Fresnel prism distortion increases towards the TIR, which blocks the shifted view beyond 5° eccentricity.

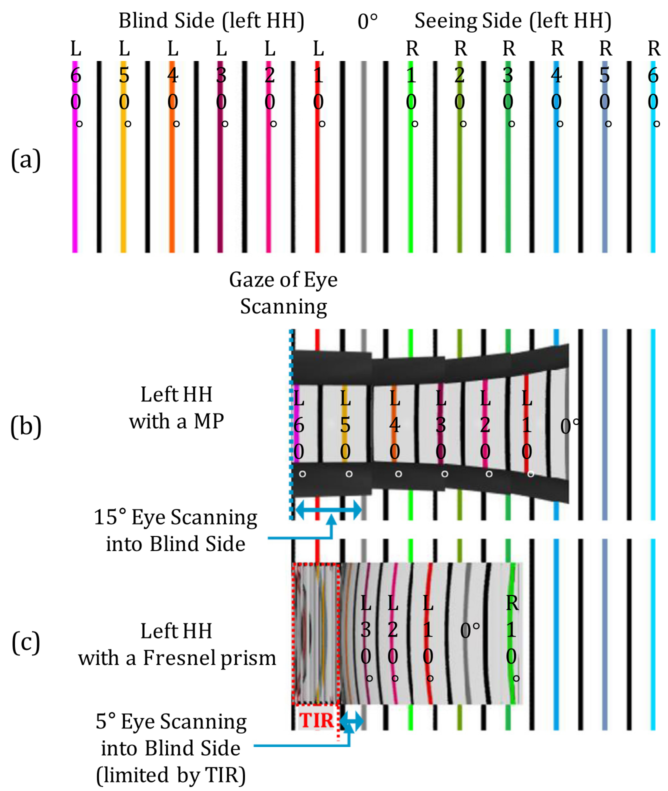

Fig. 6. Simulated monocular scene with an MP and a Fresnel prism for a patient with left HH. (a) Target scene angular pattern with different color bars in 10° steps and black bars in between. The side and eccentricities of the lines are labeled in degrees. (b) Perceived scene through the 100Δ MP. The MP was able to expand the visual field up to left 45° from the primary position of gaze and up to 57° with the 15° eye scanning into the blind side. The image is almost free of distortions. The upper and lower curved black areas are scotoma caused by the protrusion of the MP. (c) Perceived scene through the conventional 57Δ Fresnel prism. The conventional Fresnel prism provides field expansion of only 29° at the primary position of gaze and limits eye scanning range into the blind side (~5°) due to the TIR. We see dim and distorted image on approaching the TIR and spurious reflection [4] in the TIR range.

Thus, the Fresnel prism is only providing a visual field expansion of 29° with a FoV of about 34° (right 29° in seeing FoV and left 5° for additional eye scanning range). The perceived scene through the Fresnel prism has lower transmittance near the TIR (e.g., an orange bar as an indicator of 40° left). Since the height of the device's entrance pupil (toward the eye) and exit pupil (outward) are the same, the smaller angular size of the exit pupil than the entrance pupil due to its larger distance results in the protrusion scotoma as shown by black areas in Fig. 6(b). Different protrusion in each module (different distance to the exit pupil among modules) resulted in different vertical angular size of the perceived image.

To illustrate that the proposed MP would enable patients to detect possible collision we simulated images with pedestrians in the blind side (Fig. 7). A scene with three walking pedestrians at eccentricities of 29°, 41°, and 51°, as shown in Fig. 7(a), is simulated through the MP, (Fig. 7(b)), and compared with the simulated scene through the current 57Δ Fresnel prism (Fig. 7(c)).

As seen in Fig. 7(b), a left HH patient with an MP could detect the 1st and 2nd pedestrians at left 29° and 41° from the primary position of gaze and would be able to see the 3rd pedestrian at 51° left with eye scanning into the blind side. In contrast, the conventional 57Δ Fresnel prism in Fig. 7(c) only covers the 1st pedestrian at the primary position of gaze and would not present clear views of the farther 2nd or 3rd pedestrians, even with the eye scanning into the blind side due to the severe distortion followed by TIR and spurious reflection.

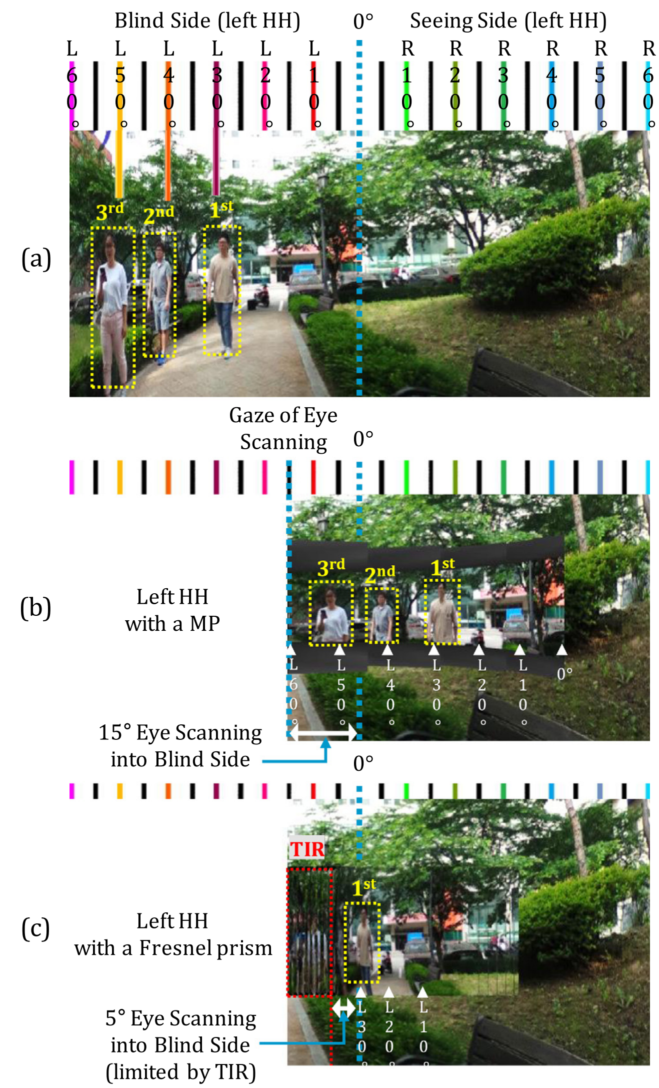

Fig. 7. Perceived view of (a) a real scene with three pedestrians at eccentricities of 29°, 41°, and 51°. To indicate the angular location, we added the horizontal angular pattern (Fig. 6a) above the scene. (b) A left HH patient could detect the first two pedestrians (highest collision risk) at the primary position of gaze and the third pedestrian in the blind side through the 100Δ MP with normal eye scanning. The upper and lower dark grey areas are scotomas caused by the protrusion of the MP. (c) With the conventional 57Δ Fresnel prism, only the 1st pedestrian would be detected the two others are not visible due to the prism distortion and TIR limitations.

In conclusion, we designed the MP and verified with ray tracing and photorealistic rendering so that our design could extend the visual field of patients with HH with a deflection power of 45° to detect the peak collision risk with other pedestrians far beyond the range of the current clinically available prism. The MP provides much better image quality, which may improve the detection performance. The MP also may be applied to patients with other types of visual field loss, such as tunnel vision [5,6]. The potential functionality of the device was demonstrated by optical simulation. The protrusion scotoma (upper and lower black areas in Figs. 6(b) and 7(b)) are due to the different angular size of the entrance and exit pupils of the device and can be resolved by further developments.

Funding sources

This research was supported by National Institute of Health, USA (R01EY23385) and Basic Science Research Program through the National Research Foundation of Korea funded by the Ministry of Education, Republic of Korea (NRF-2018R1D1A1B07049563)

References

[1] H. Apfelbaum, E. Peli, Tunnel vision prismatic field expansion: Challenges and requirements, Transl. Vis. Sci. Technol. 4 (2015) 8.

[2] C. Qiu, J.-H. Jung, M. Tuccar-Burak, L. Spano, R. Goldstein, E. Peli, Measuring pedestrian collision detection with peripheral field loss and the impact of peripheral prisms, Transl. Vis. Sci. Technol. 7 (2018) 1.

[3] J.M. Cohen, An overview of enhancement techniques for peripheral field loss, J. Am. Optom. Assoc. 64 (1993) 60.

[4] E. Peli, Field expansion for homonymous hemianopia by optically-induced peripheral exotropia, Optom. Vis. Sci. 77 (2000) 453.

[5] H. Apfelbaum, N.C. Ross, A.B. Bowers, E. Peli, Considering apical scotomas, confusion, and diplopia when prescribing prisms for homonymous hemianopia, Transl. Vis. Sci. Technol. 2 (2013) 2.

[6] J.-H. Jung, E. Peli, Impact of high power and angle of incidence on prism corrections for visual field loss, Opt. Eng. 53 (2014) 061707.

[7] K.E. Houston, E. Peli, R.B. Goldstein, A.R. Bowers, Driving with hemianopia VI: Peripheral prisms and perceptual-motor training improve blind-side detection in a driving simulator, Transl. Vis. Sci. Technol. 7 (2018) 5.

[8] A.T. Bahill, D. Adler, L. Stark, Most naturally occurring human saccades have magnitudes of 15 degrees or less, Investig. Ophthalmol. 14 (1975) 468.

[9] E. Peli, A.R. Bowers, K. Keeney, J.-H. Jung, High-power prismatic devices for oblique peripheral prisms, Optom. Vis. Sci. 93 (2016) 521.

[10] E. Peli, H. Apfelbaum, E.L. Berson, R.B. Goldstein, The risk of pedestrian collisions with peripheral visual field loss, J. Vis. 16 (2016) 1.

[11] M. Katz, Visual acuity through Fresnel, refractive, and hybrid diffractive/refractive prisms, Optometry 75 (2004) 503.

[12] H. Gross, F. Blechinger, B. Achtner, Human eye, in: H. Gross (Ed.), Handbook of Optical Systems, Volume 4: Survey of Optical Instruments, Wiley-VCH Verlag GmBH & Co., KGaA, Weinheim, Germany, 2008.

[13] J.-H. Jung, E. Peli, Field expansion for acquired monocular vision using a multiplexing prism, Optom. Vis. Sci. 95 (2018) 814.